pg 2017 to 2022 in Vol 2 of Proceedings
title page attached

MERCURY POROSIMETRY STUDIES ON A NATURAL FRACTURE

L.R. Myer, A.M. Cook-Polak,
Earth Sciences Division
Lawrence Berkeley Laboratory
University of California
Berkeley, CA 94720
(510) 486-6456

L.J. Pyrak-Nolte and
Purdue University
West Lafayette, IN 47907
(317) 494-3258
(617) 253-4352

C. Marone
Massachusetts Institute of
Technology
Cambridge, MA 02139

INTRODUCTION

Of central importance to the evaluation of the suitability of an unsaturated site for disposal of nuclear waste is the potential for transport through natural fractures. While model studies continue to be performed to evaluate the importance of fractures there remains considerable uncertainty regarding the actual capillary pressure and relative permeability properties of natural fractures. Of particular importance is the effect of stress on two-phase flow properties. While two-phase flow is relatively insensitive to the stress state in porous media, results of this study show that both capillary pressure characteristics and relative permeability could be very dependent upon the in-situ stress conditions. Model results further show that the stress effects can arise from elastic deformations in the fracture.

DESCRIPTION OF EXPERIMENTS

In this study mercury porosimetry techniques were used to study the effects of stress on the capillary pressure characteristics of a single natural fracture. In addition, permeability measurements were made with mercury as the flowing fluid.

The sample used in this experiment was a section of granite core of diameter 11.54 cm with a single natural fracture through it, roughly normal to the core axis. To keep the mercury from leaking out of the fracture, a nylon jacket was glued around the sample and a steel jacket was fitted over the nylon jacket to provide additional confinement. Two ports were provided for entry and exit of the mercury.

The experimental set-up consisted of a reservoir to hold the mercury, an inlet capillary tube to measure the volume of mercury that flowed into and out of the fracture, and an exit capillary tube to measure the flow rate of mercury across the fracture (Figure 1). The reservoir and the two capillary tubes were connected to each other and to the sample by means of 3.2 mm diameter, high-pressure, clear plastic tubing. The mercury in the reservoir, capillary tubes, and high-pressure tubing was kept under a constant injection pressure using nitrogen gas. The capillary tubes used to measure mercury volume changes and flow rates had an inside diameter of 0.5 mm, permitting resolution of volume changes as small as 2×10^{-10} m^3.

Tests were carried out over a range of load conditions and mercury injection, or capillary, pressures. The injection pressures used were 0.1, 0.2, 0.4, and 0.8 MPa. For each injection pressure, the sample was subjected to a vertical (normal to the fracture plane) loading sequence, with measurements of mercury volume change and flow being carried out at axial stresses of 2.8, 5.7, 11.4, 17.1, 22.8, and 47.6 MPa. The sample was first loaded to the maximum axial stress level, then unloaded sequentially to the minimum levels and finally loaded again through the reverse sequence back to maximum.

MERCURY VOLUME CHANGE MEASUREMENTS

Figure 2 shows the mercury volume changes measured during the tests. Each curve represents only the volume change due to the change in axial load at one value of mercury injection pressure. The injection pressure was increased after each cycle while the sample was under 47.6 MPa axial stress.

The additional mercury which entered the fracture upon increasing the mercury pressure at 47.6 MPa axial stress was small compared to subsequent changes during the loading cycle and could not accurately be distinguished from apparent volume changes due to the compliance of the tubing, etc. Therefore the initial mercury volume at the beginning of a loading cycle at a new mercury pressure was set equal to the volume at the end of the previous load cycle.

The data in Figure 2 can be used first of all to estimate the sizes of the voids present in the fracture and the effect of changing stress on the size of the voids. The relationship between mercury injection pressure, P, and pore radius, r, is given by Laplaces equation:

$$P = 2\frac{T}{r}\cos\alpha \qquad (1)$$

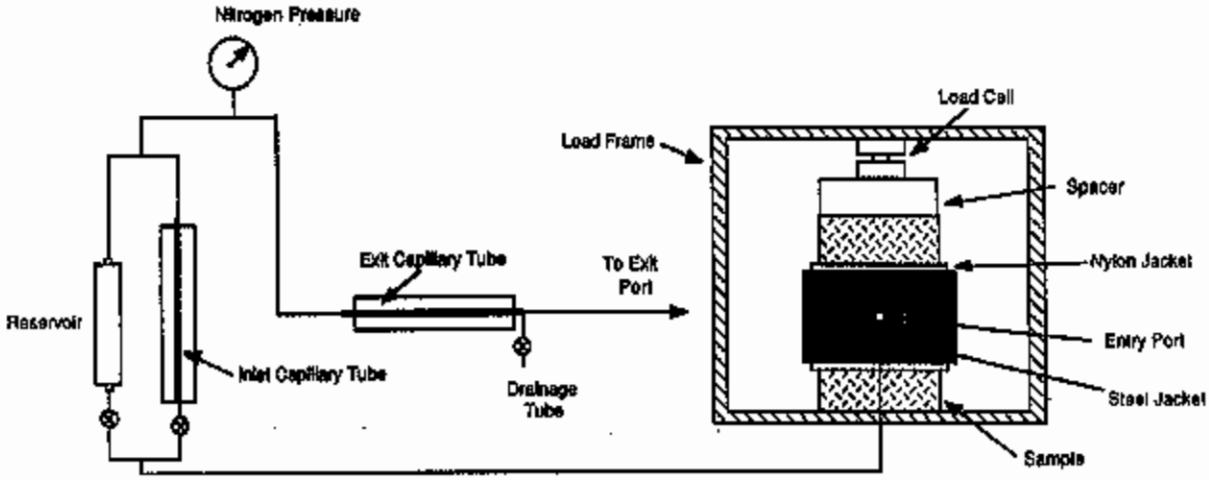

Figure 1 Schematic illustration of experimental apparatus.

where T is surface tension, alpha is the contact angle and it is assumed that a pore is represented by a cylindrical tube of radius r or a flat void with sides separated by a distance 2r. Using Equation (1) the data shown in Figure 2 indicate that the process of unloading the sample from an axial stress of approximately 48 MPa to 3 MPa resulted in opening of voids with apertures ranging from at least 1 μm to 19 μm. Hysteresis is also observed in the curves in Figure 2; that is, when the axial stress was increased from 3 MPa back to 48 MPa, less mercury came out of the fracture than had gone in. The hysteresis is due to entrapment of mercury by necks located along flow paths. The amount of hysteresis exhibited during the cycle at 0.8 MPa mercury pressure is suspect because a leak developed in the experimental system during the cycle, permitting loss of an unknown amount of mercury. This loss could account for a significant portion of the hysteresis at this mercury pressure.

Each of the curves in Figure 1 also shows that, at any capillary pressure, the volume injected increases nonlinearly with decreasing axial stress. This means that the number of voids exceeding a certain aperture increased as the stress decreased. The implication of observations of changing void size and numbers of voids is that not one, but a family of curves is required to represent the capillary pressures characteristics of a fracture. Thus capillary pressures required for model studies need to be functions of stress as well as saturation state.

Modelling Volume Change

Results of the porosimetry measurements were modeled to help understand the mechanisms responsible for the observed behavior. The model assumes the rock is linearly elastic. Therefore, under changing normal stress, the average mechanical displacement, $d_{(mech)}$, of the fracture integrated over the plan area of the fracture must be equal to the change in void volume of the fracture. Average mechanical displacement is that which would be measured by a gauge spanning a fracture minus the displacement associated with

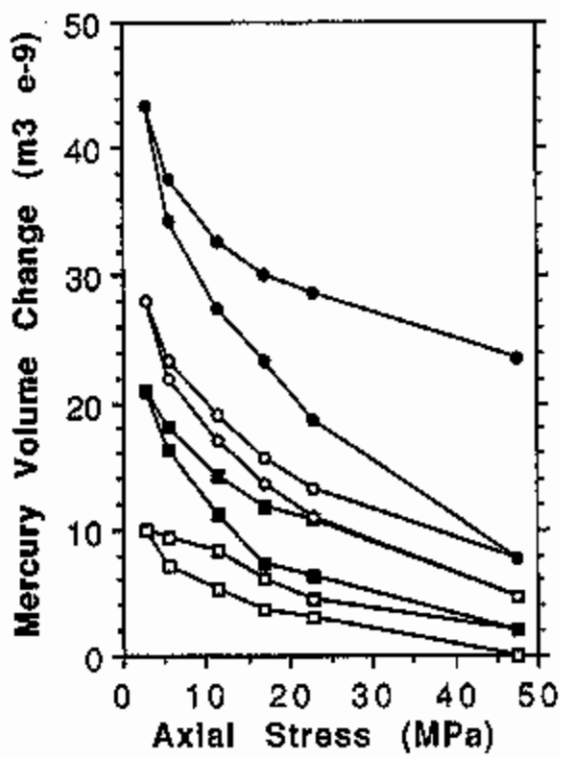

Figure 2 Mercury volume change as a function of normal stress applied to a single natural granite fracture.

elastic deformation of the intact rock. As a first order assumption the volumetric change is distributed equally among all apertures. Thus changes in mechanical displacement, $\delta(d_{mech})$, may be related to changes in void aperture, $\delta(d_{void})$, through the ratio of void space area to the cross-sectional area of the fracture plane:

$$\delta(d_{mech}) = A_{void}/A \ \delta(d_{void}). \qquad (2)$$

Where A_{void} is the void space cross-sectional area and thus varies with d_{void}, and A is the nominal cross-sectional area of the fracture plane. Summing the void area for all apertures shows that the maximum far-field fracture displacement d_{max} is simply the ratio of void volume V_{void} to cross-sectional area:[1]

$$d_{max} = d_{mech}(\infty) = Vvoid/A \qquad (3)$$

Global accessibility was assumed, so the volume of "mercury" in the model at any injection pressure was calculated from the number of apertures larger than the minimum non-wetting aperture for the applied injection pressure. The model accepted as input the aperture distribution present in the fracture at the lowest normal stress level used in the tests. Additional assumptions were that all voids were filled at a capillary pressure of 0.8 MPa and all voids were closed at the highest axial stress of 47.6 MPa.

Two corrections were applied to the data to make it more compatible with the first order model. As noted above, mercury was trapped during a loading/unloading cycle. Thus, upon subsequent cycles, some mercury was already present from the previous cycle. For comparison with the model, this means that the void volume measurements were too small. This effect was corrected for by using the following relation:

$$V_c^i = V_o^i + V_h^i\,(1-d/d_{max}) \qquad (4)$$

where V_c^i is the corrected volume at normal load i, V_o^i is the measured volume at normal load i, and V_h^i is the volume of Hg trapped in voids (as given by the magnitude of the hysteresis loop at 47 MPa.), and d/d_{max} is the normalized closure.

The second correction consisted of displacing all data curves downward so that first point on the unloading curve at 47.6 MPa was at zero. This was done to be consistent with the model assumption that all voids were closed at this highest axial stress. The corrected data are replotted in Figure 3. In part b of the figure the data have been normalized by dividing the measured volumes by the volume of mercury (38.7×10^{-9} m^3) at the highest capillary pressure and lowest axial stress. Using equations 2 and 3, and assuming all voids were filled at 0.8 MPa mercury pressure, the fracture displacement corresponding to each stress level was determined, so that the measured mercury

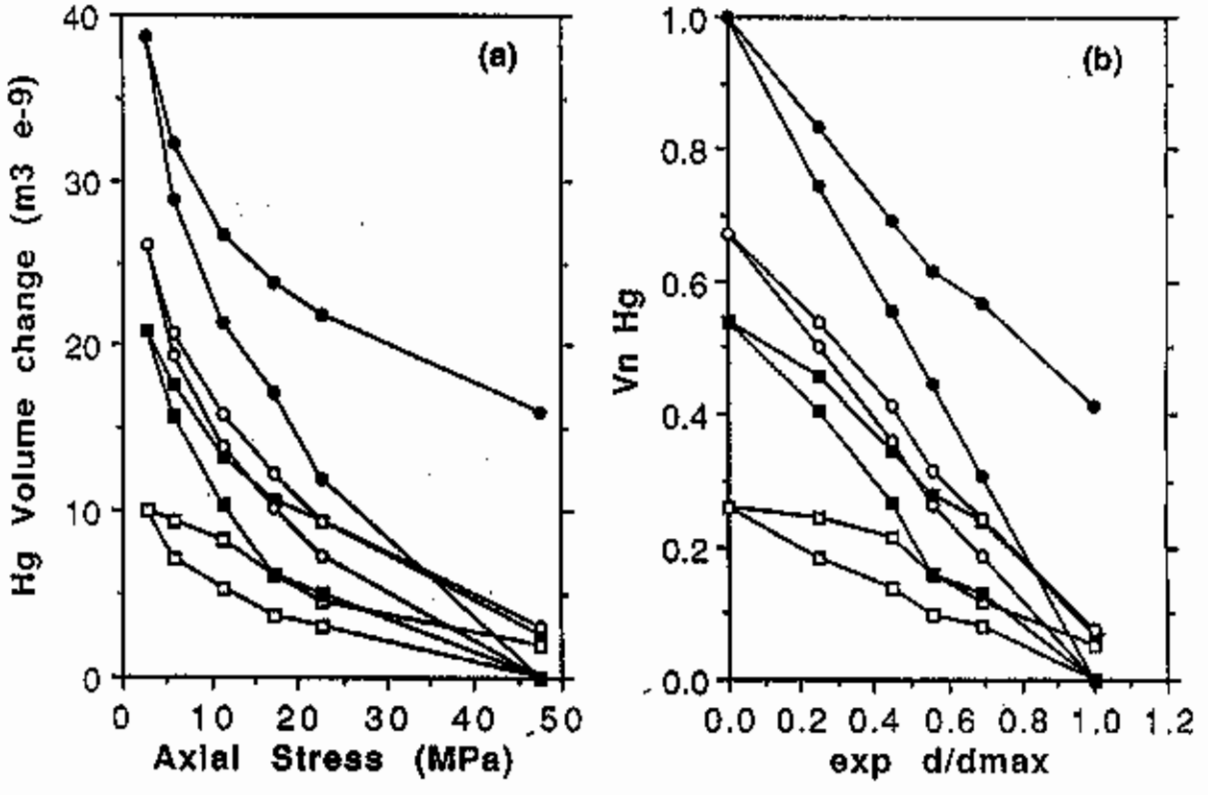

Figure 3 Measured mercury volume change after corrections to data presented as a function of stress on the fracture in a, and, in part b, normalized and presented as a function of normalized fracture closure, d/dmax.

volume changes could be plotted as a function of fracture displacement.

On the assumption that all void space within the fracture accessed at the highest capillary pressure, the data for capillary pressure of 0.8 MPa define a straight line when plotted as normalized void volume vs normalized fracture closure. Deviations from this line at lower capillary pressures reflect incomplete filling of the fracture voids by the non-wetting fluid.

Theoretical curves of fracture closure (normalized fracture volume vs. d/d_{max}) were calculated from aperture-frequency distributions using Equation (2). We calculate the normalized fracture volume, V, and closure, d, by simply incrementing d_{void} from 0 to the maximum aperture assuming unit cross-sectional area for voids of all aperture. Thus, V_{void}/A and A_{void}/A are obtained from the aperture distribution according to:

$$V_{void}/A = ISU\ (i=d_{void},\ i_{max},\ i\ f(i)) \qquad (5)$$

$$A_{void}/A = ISU\ (i=d_{void},\ i_{max},\ f(i)) \qquad (6)$$

where f(i) is the frequency of voids of aperture i and d_{void} denotes aperture closure. Both equations are a function of fracture closure d_{void}. Thus f(0) denotes the contact area when the fracture surfaces just come into contact and $f(i_{max})$ is the normalized number of apertures of height i. The value d_{max} is given by Equation (3) with d_{void}=1.

Equations 2-6 are used together to produce closure curves of normalized fracture volume vs. normalized displacement. The theoretically calculated volume of mercury at each injection pressure and axial stress state is found by subtracting the volume of voids smaller than the minimum non-wetting aperture from the total void volume. Values of apertures in the model are unitless. However, to be consistent with the principal expressed by Laplace's equation, the minimum non-wetting aperture assumed in the model decreases by a factor of two for each factor of two increase in mercury pressure.

The aperture distribution input to the model was derived from the experimental mercury volume data at each value of fracture closure. For example, assuming a minimum nonwetting aperture of 2 at a capillary pressure of 0.8 MPa, the four data points at a closure of d/dmax=0 imply that 33% of the volume is contained in apertures of sizes 2-3, 13% between 4 and 8, 28% between 8 and 16, and 26% between 16 and 32. An aperture distribution may be defined for the set of data points at each d/dma_x using the following relation:

$$f(i) = \frac{[V(k+1) - V(k)]/N(j)}{A(i)} \quad (\text{for } k=0 \text{ to } 3 \text{ and } j=0 \text{ to } 4) \qquad (7)$$

Where k is an index for capillary pressure, running from 3 at 0.8 MPa to 0 at 0.1 MPa, N(j) is the range of apertures between the points at each capillary pressure (as in the above example), and the other parameters have the same meaning as above. In this case, an aperture distribution is derived for each j. Thus five distributions are possible (we neglect the points at d/d_{max}=1). They are normalized to give unit fracture volume, as discussed above. As shown in Figure 4, the distributions are quite similar, each showing a large percentage of small apertures. Using

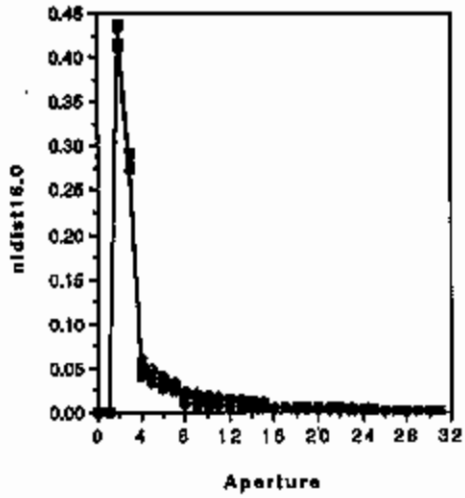

Figure 4 Normalized aperture distributions derived from the data at each d/dmax; the five distributions are almost indistinguishable.

these aperture distribution the fracture was "closed" and mercury volumes were calculated as discussed above for comparison with experimental values.

Results using the frequency distribution derived from the data at the lowest axial stress are compared with experimental measurements in Figure 5. Because trapping is not included in the model, model predictions would be the same for both the loading and unloading of the fracture. The model is a better fit to the experimental data obtained during the loading portion of the test for mercury pressures less than 0.8 MPa, and it is this data which is presented in the figure. Results are in reasonable agreement with the model predictions in that the flattening of the curves as mercury pressure is reduced, and the spacing between curves at the various values of fracture closure are represented by the model.

The agreement between results of the modelling and experimental observations showed that the effects of stress on capillary pressure characteristics of the natural granite fracture were due to elastic deformation and subsequent changes in void size and distribution. Analyses also showed that the model results were very sensitive to the shape of the void frequency distribution function. By a trial and error procedure a number of different distributions were tried, all of which resulted in poor agreement with observations. Having data at different mercury injection pressures and different stress levels placed significant constraints on the form of the distribution required to fit the data.

Mercury Flow Measurements

The permeability of the fracture to mercury was measured as a function of stress at each mercury injection pressure. The flow measurements were performed after equilibrium was attained at the axial stress/capillary pressure state. A small additional head of mercury (20 or 75 cm) was then applied at the injection port and the volume flow per unit time measured in the exit capillary tube after steady state flow conditions were obtained. The volume data were plotted against time for all

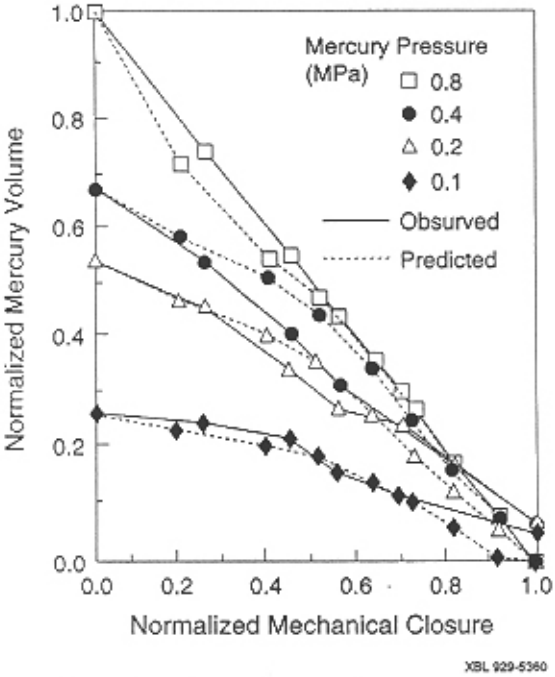

Figure 5 Comparison of measured mercury volume change with predictions based on elastic deformations in fracture and no trapping.

loads in the unloading and loading sequences and at all injection pressures. The slope for each curve was divided by the pressure gradient to normalize the flow rates. These normalized flow rates, Q, were plotted against load to evaluate the effects of normal stress and injection pressure. Results plotted in Figure 6 show that there is a considerable difference between flow behavior at a mercury pressure of 0.8 MPa and that at lower pressure. The rapid reduction in flow with stress at the 0.8 MPa mercury pressure is similar to what would be expected if a wetting fluid were flowing under saturated conditions.[2] However, at lower mercury pressures the change in flow with stress was much less pronounced. The resemblance of the results at 0.8 MPa mercury pressure to saturated wetting phase flow is understandable since the fracture was nearly 100% saturated at this mercury pressure. At lower mercury pressures the small apertures, which also rapidly close with increasing stress, are eliminated by capillary pressure restriction, from the connected flow path.

In Figure 7 the flow data are combined with the volume-change data to produce plots of permeability as a function of percent saturation in the fracture. Values of percent saturation were obtained by assuming, as was done above, that the volume of mercury in the fracture at each axial stress level during unloading at an injection pressure of 0.8 MPa represented 100% saturation of the fracture. Saturation levels at each axial stress level were determined by dividing the volume measurements by the mercury volume at P = 0.8 MPa. Because mercury is nonwetting, these curves represent the relative permeability of the fracture to the nonwetting liquid.

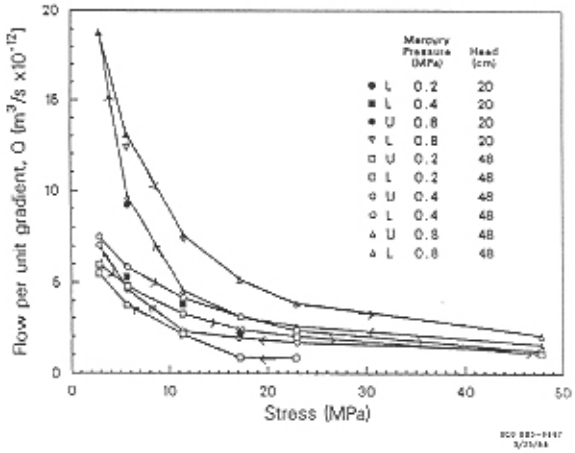

Figure 6 Measured mercury flow as a function of stress on the fracture; arrows represent loading direction, L refers to loading and U to unloading, mercury pressure is the capillary pressure during testing and the head of mercury applied is given in centimeters.

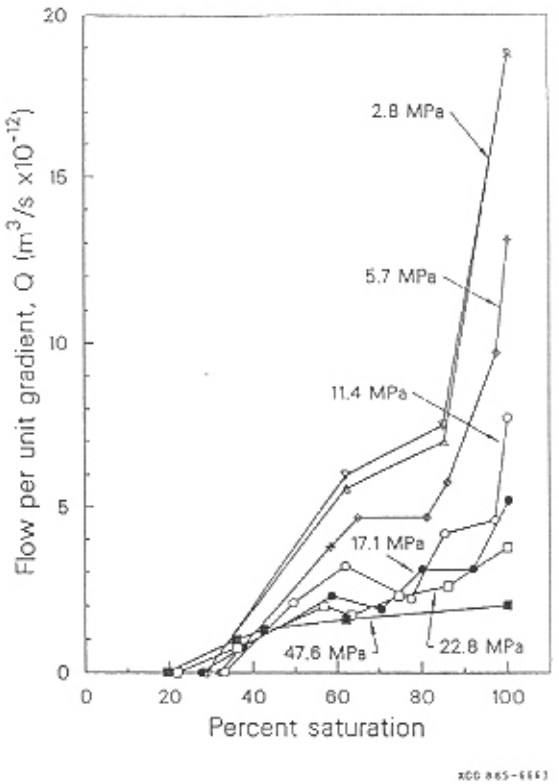

Figure 7 Permeability of the fracture to mercury as a function of mercury saturation and normal stress on the fracture.

The general shape of the curves appears similar to the relative permeability curves often obtained for porous media, however, there are significant differences between the curves at different stress levels. This shows that, in general, there is not a unique relationship between the relative permeability of fractures and saturation levels if stress conditions are changing. In addition, at low normal stresses the reduction in non-wetting phase permeability with decreasing saturation occurs much more rapidly than at high stress levels. It is also significant that at a saturation of about 20-35% there was no flow. Even though mercury entered the fracture, a connected path between inlet and outlet was not present.

These results further suggest that the changes in geometry of fracture voids, and, in particular, the presence of critical necks along the flow path have a dominant effect on the two phase flow behavior in a single fracture.

CONCLUSIONS

The voids of a fracture form an interconnected network through which fluid must flow. Mercury porosimetry techniques can be used to explore the two-phase flow properties of this network in much the same way as is commonly done in porous rocks. However, fracture voids tend to be more crack-like in shape compared to the more equant-shaped pores in a porous rock. Since crack-like shaped voids deform more easily under applied stress, the two phase flow properties of fractures are subject to a much higher degree of stress sensitivity than porous media. This stress sensitivity has been observed in capillary pressure and non-wetting phase permeability measurements on a natural granitic fracture. Results show that capillary pressure and relative permeability expressions for fractures are functions of stress state as well as saturation state, and could significantly influence results of flow and transport modelling in unsaturated fractured rock.

ACKNOWLEDGMENTS

This work was supported by the Manager, Chicago Operations, Repository Technology Program, Repository Technology and Transportation Division, Director, Office of Civilian Radioactive Waste Management Office of Facilities Siting and Development, Siting and Facilities Technology Division, and by the Assistant Secretary for Energy Research, Office of Basic Energy Sciences, Division of Engineering and Geosciences, of the US Department of Energy under Contract No. DE-AC03-76SF00098.

REFERENCES

1. L.J. PYRAK-NOLTE, N.G.W. COOK, AND D. NOLTE, "Fluid percolation through single fractures," Geophysical Research Letters, Vol 15, No 11, pgs 1247-1250, (1988).

2. L.J. PYRAK-NOLTE, L.R. MYER, N.G.W. COOK, and R. A. WITHERSPOON, "Hydraulic and mechanical properties of natural fractures in low permeability rock", Proceedings of 6th International Congress of Rock Mechanics, Montreal, I, 225-232, 1987.

VOLUME 1
1993

HIGH LEVEL RADIOACTIVE WASTE MANAGEMENT

Proceedings of the Fourth Annual International Conference Las Vegas, Nevada, April 26-30, 1993

Sponsored by the
American Society of Civil Engineers
American Nuclear Society

in cooperation with

American Chemical Society
American Institute of Chemical Engineers
American Medical Association
American Society for Testing and Materials
American Society for Quality Control
American Society of Mechanical Engineers
Center for Nuclear Waste Regulatory Analysis
Edison Electric Institute
Geological Society of America
Health Physics Society
Institute of Nuclear Materials Management
National Conference of State Legislatures
Society of Mining Engineers
U.S. Department of Energy
U.S. Nuclear Regulatory Commission
University of Nevada Medical School
American Association of Engineering Societies
American Institute of Mining,
Metallurgical, and Petroleum Engineers
American Underground - Space Association
Atomic Energy Council Radwaste Administration
Atomic Energy of Canada Ltd.
British Nuclear Fuels Ltd.
Chinese Institute of Civil and Hydraulic Engineering
Commission of the European Communities
Conseil National des Ingenieurs et des Scientifiques de France
Electric Power Research Institute
Her Majesty's Inspectorate of Pollution
Institution of Civil Engineers
Institution of Engineers — Australia
Institution of Engineers of Ireland
Japan Society of Civil Engineers
Korea Advanced Energy Research Institute
Korean Society of Civil Engineers
Nationale Genossenschaft fur die Lagerung Radioaktiver Abfälle (NAGRA)
National Society of Professional Engineers
Organization for Economic Cooperation and Development (OECD) — Nuclear Energy Agency
Power Reactor and Nuclear Fuel Development Corporation
Swedish Nuclear Fuel and Waste Management Company
Swedish Nuclear Power Inspectorate
Swiss Society of Engineers and Architects
Verein Deutscher Ingenieure
Ministerio de Industria y Energia-Uruguay

Hosted by the

University of Nevada, Las Vegas
Howard R. Hughes College of Engineering

Published by the

American Nuclear Society, Inc.
La Grange Park, Illinois 60525, USA
American Society of Civil Engineers
New York, New York 10017-2398, USA